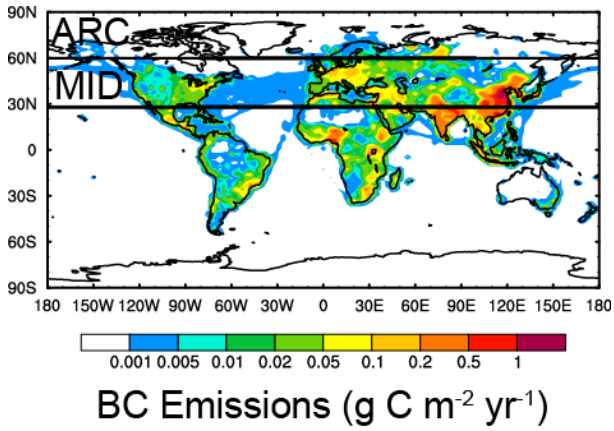

Figure S1. Spatial distribution of annual anthropogenic emissions (g C m^{-2} yr^{-1}) of black carbon (BC) averaged over 2008–2012. The geographical source regions for emission perturbations in this study are the Arctic (ARC; 60–90°N) and mid-latitudes (MID; 28–60°N).

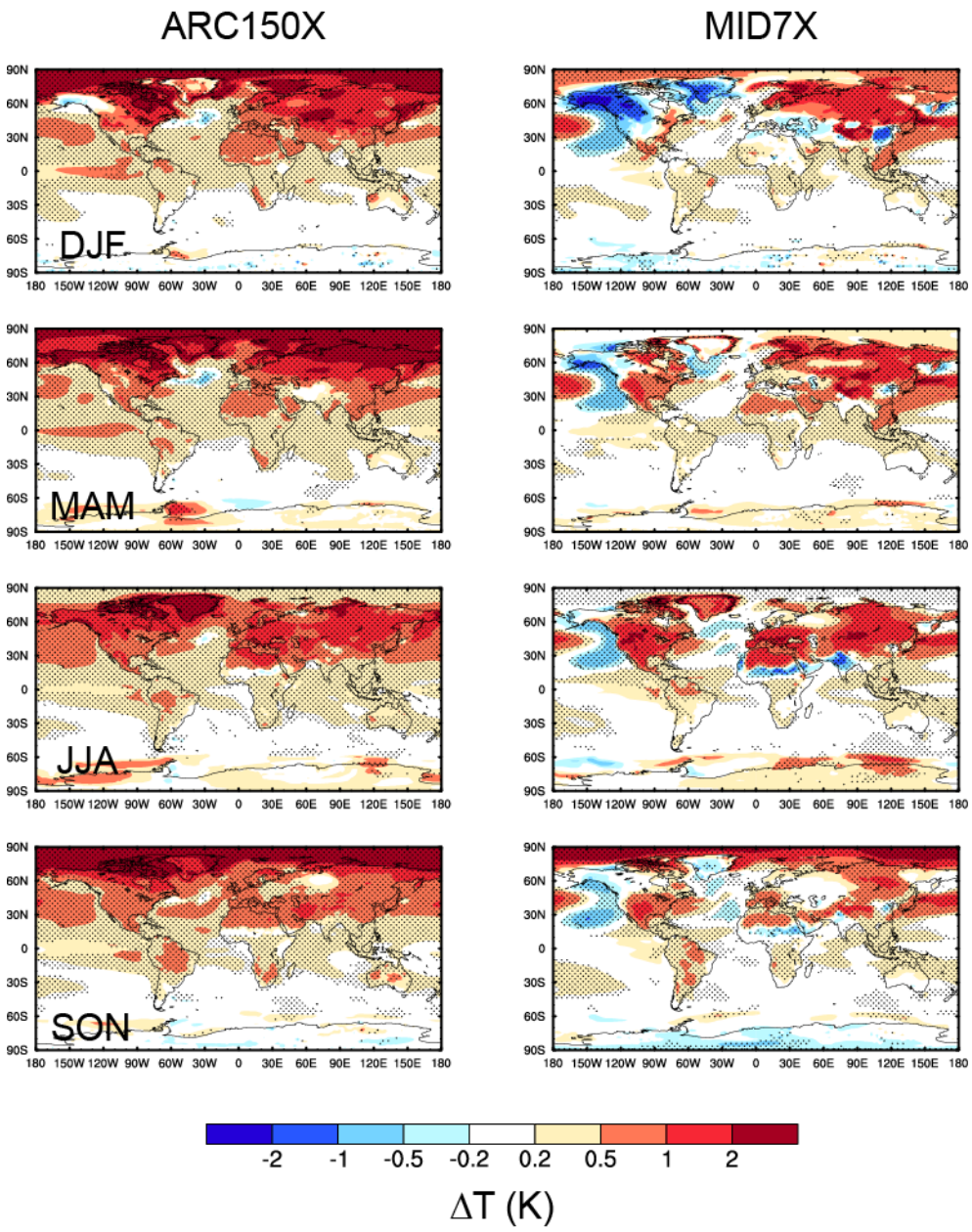

Figure S2. Spatial distribution of changes in December-January-February (DJF), March-April-May (MAM), June-July-August (JJA) and September-October-November (SON) (from top to bottom) mean surface air temperature (K) for ARC150X (left) and MID7X (right) compared to PD. The dotted areas indicate statistical significance with 95% confidence from a two-tailed Student's t test.

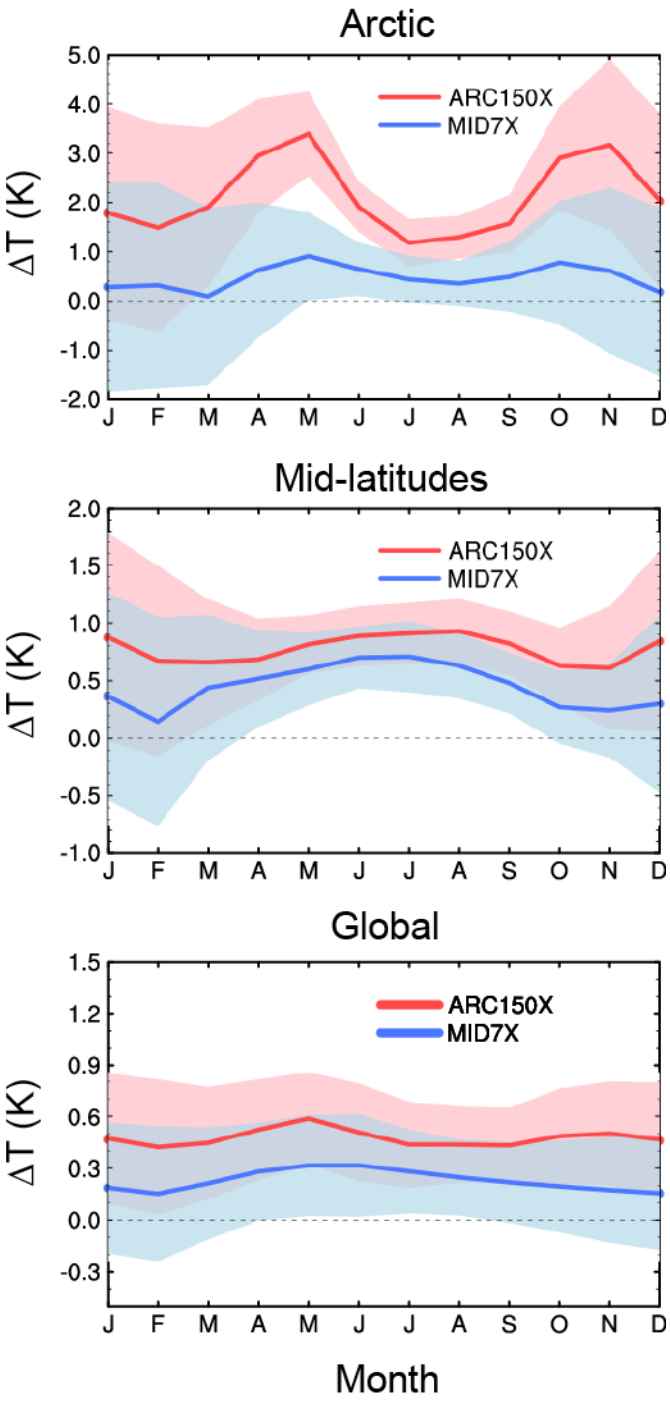

Figure S3. Changes in Arctic (top), mid-latitude (middle) and global (bottom) monthly mean surface temperature (K) for ARC150X/MID7X compared to PD.

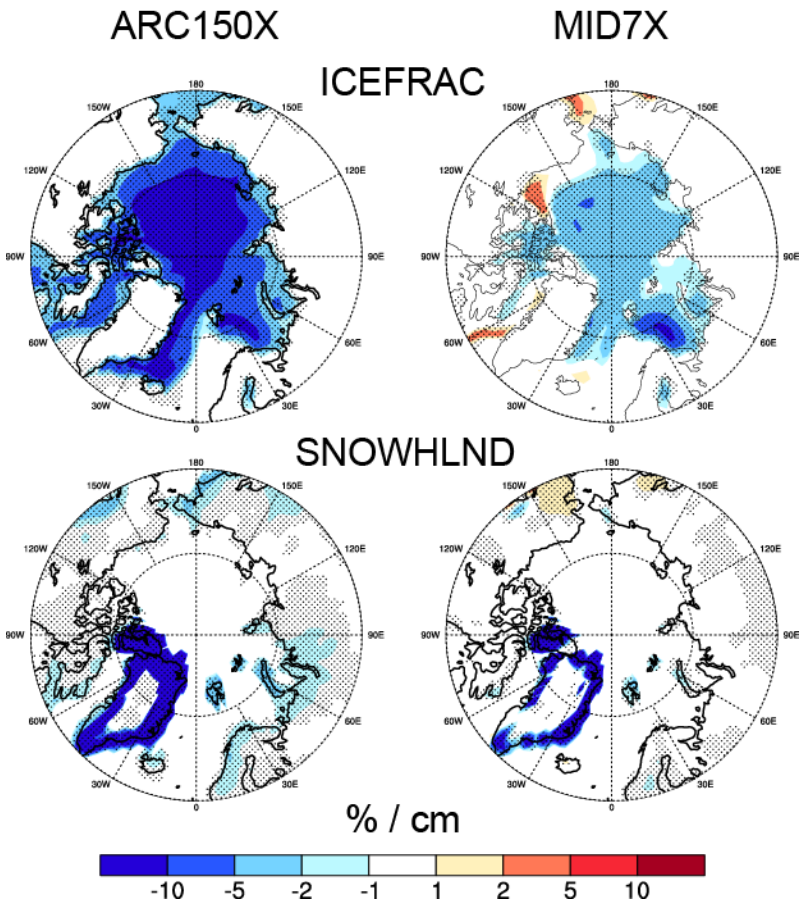

Figure S4. Changes in annual and zonal mean fraction of surface area covered by sea-ice (ICEFRAC, %, top) and water equivalent snow depth over land (SNOWHLND, cm, bottom) for ARC150X (left) and MID7X (right) compared to PD.

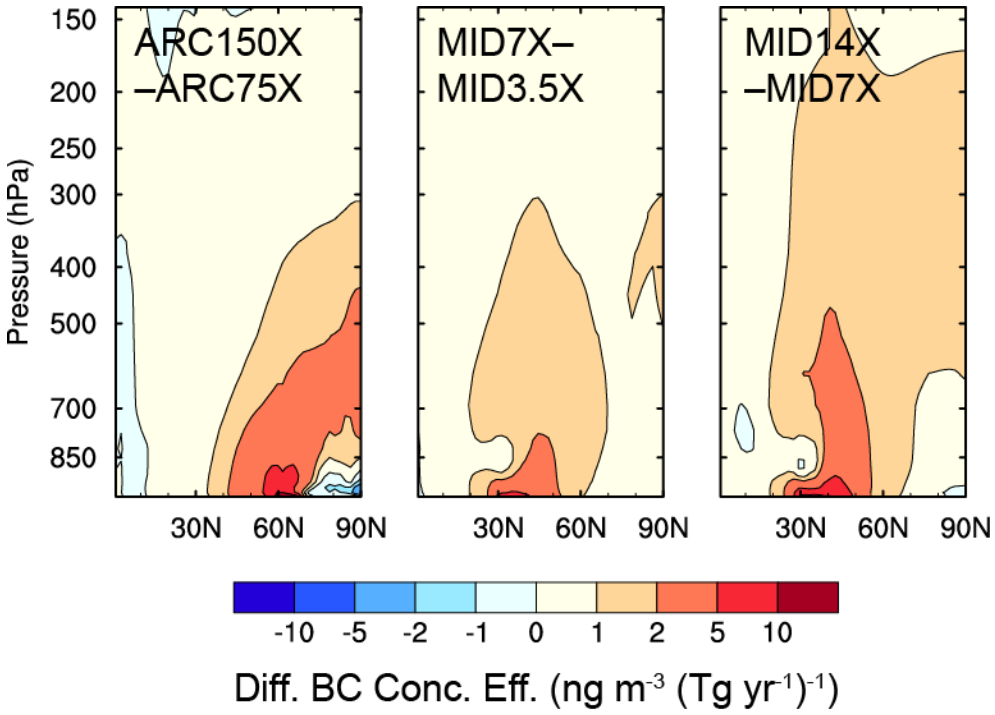

Figure S5. Differences in annual and zonal mean BC concentration efficiency (ng m^{-3} (Tg yr^{-1}) $^{-1}$) between ARC150X and ARC75X (left), MID7X and MID3.5X (middle), and MID14X and MID7X (Right).

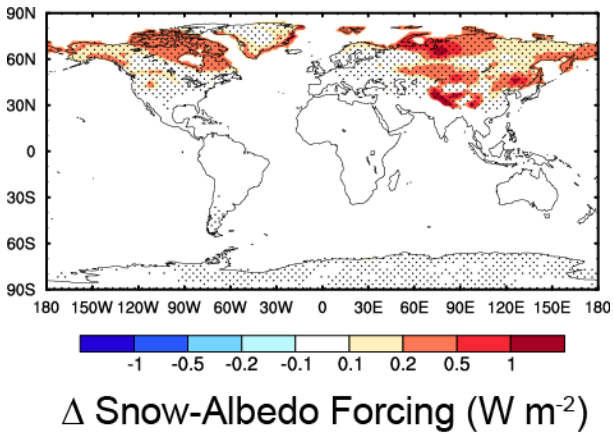

Figure S6. Spatial distribution of snow/ice-albedo forcing of BC (W m^{-2}) between PD and PI.